ASTRONOMY & ASTROPHYSICS
SUPPLEMENT SERIES

AUGUST **1998**, PAGE 209

Astron. Astrophys. Suppl. Ser. **131**, 209–219 (1998)

Broad-band $JHK(L')$ photometry of a sample of giants with $0.5 > [\mathrm{Fe/H}] > -3$

A. Alonso, S. Arribas, and C. Martínez-Roger

Instituto de Astrofísica de Canarias, E-38200 La Laguna, Tenerife, Spain
e-mail: aas@ll.iac.es, sam@ll.iac.es and cmr@ll.iac.es

Received August 14, 1997; accepted February 23, 1998

Abstract. We present the results of a three-year campaign of broad-band photometry in the near-infrared J, H, K and L' bands for a sample of approximately 250 giant stars carried out at the Observatorio del Teide (Tenerife, Spain). Transformations of the Telescopio Carlos Sánchez system into/from several currently used infrared systems are extended to the redward part of the colour axis. The linearity of our photometric system in the range -3 mag $< K <$ 10.5 mag is inferred from the intercomparison of data of stars common to this and other photometric systems. A preliminary assessment of the photometric extinction profile of the Observatorio del Teide in $JHKL'$ is also provided.

These observations are a continuation of a programme aimed towards the progressive completion of a whole grid of $T_{\rm eff}-[\mathrm{Fe/H}]-\log(g)$–colour relations for population I and II stars. The analysis of optical and IR colour-colour diagrams reveals that the range F0III−K5III is well sampled for $0.5 > [\mathrm{Fe/H}] > -3$. Data of comparable quality previously published have been added to the sample in order to increase the reliability of the relations to be obtained. We also provide mean IR colours for giant stars according to spectral type[1].

Key words: stars: population II — infrared: stars — stars: general — stars: fundamental parameters

1. Introduction

The precise relationships which link the physical parameters of stellar atmospheres (i.e. $T_{\rm eff}$, $\log(g)$ and [Fe/H]) with measured colours, photometric indices or spectral features of stars play a central role connecting several areas of stellar physics. In particular, the accurate calibration of the scale of stellar effective temperatures is of increasing importance in spectroscopic studies since $T_{\rm eff}$-colour or -spectral type calibrations are usually adopted in deriving chemical abundances. On the one hand, noteworthy differences in the derived ratios between different elements are obtained when analysing the same spectra with different temperature scales (e.g. King 1994), thus implying quite different scenarios for the chemical evolution of the galaxy. On the other hand, non-negligible variations in primordial abundances may be deduced from the adoption of diverse temperature scales in spectroscopic analysis (e.g. Bonifacio & Molaro 1997). Stellar effective temperatures are also a most influential consideration in the observed differences of the giant branch and main sequence slopes when comparing empirical lines of globular clusters with theoretical isochrones (e.g. Bell 1992). Here a part of the discrepancy might be induced by the adoption of an incorrect temperature scale (since this is crucial in the transformation of the HR diagram from the theoretical to the observational plane). Furthermore, the effective temperature scale is necessary for the analysis of the global behaviour of stellar atmosphere models (e.g. Castelli et al 1997), in particular it is a relevant parameter for the modelling of molecular bands in the synthesis of infrared colours (e.g. Bell & Gustafsson 1989). Finally, it is also important for the overall colour synthesis of stellar populations (e.g. Vazdekis et al. 1996).

We have carried out these observations as a part of a continuing programme aimed at the (semi-)empirical calibration of $T_{\rm eff}$ as a function of photometric colours, [Fe/H] and $\log(g)$ for population I and II stars. The part of the programme concerning stars with $\log(g) \gtrsim 3.5$ (i.e. the main sequence and the blue part of subgiant branch) has been recently accomplished, and is described in Alonso

Send offprint requests to: A. Alonso

[1] Tables 1, 2 and 3 are only available in electronic form via the CDS (anonymous ftp 130.79.128.5 or http://cdsweb.u-strasbg.fr/Abstract.html

et al. (1996a,b; Papers III and IV respectively). As for the part of the programme devoted to the giant branch temperature scale, we have selected a sample of ∼400 stars with spectral types from F0 to K5 covering a wide range in metal content ($+0.5 > [Fe/H] > -3.0$). In order to obtain their effective temperatures, we will apply the Infrared Flux Method (Blackwell et al. 1990), which has proved useful for deriving stellar effective temperatures of metal-poor giants of globular clusters (Arribas & Martínez-Roger 1987a; Arribas et al. 1991). Furthermore, this method relies only weakly on theoretical models and its main requirement from the observational side is the measurement of accurate photometry needed to derive near infrared monochromatic fluxes. In this paper, we present and discuss the results of the observational campaign of near-IR photometry for the stars of the sample lacking previously measured $JHK(L')$ magnitudes, and also for stars common to other systems which will be necessary to homogenize the photometric measurements taken from the literature. The infrared magnitudes will be used in a later stage of the work to derive IR monochromatic fluxes for the application of the Infrared Flux Method.

2. Selection of the sample

We have searched the literature in order to collect a sample of giant stars representative of the different populations in our Galaxy. The main criteria imposed on the search,without order of priority, were determined by the final aim of the programme (i.e. photometric calibration of the effective temperature scale) and were that the stars should:

a) have published $UBV(RI)$ and *uvby* photometry,

b) have determined or estimated metal abundance,

d) be preferably close to the solar neighbourhood, in order to avoid large interstellar reddening, which biases the analysis of temperatures,

d) have (at least tentative) spectral type determinations, and

e) be contained in the input catalogue of *Hipparcos*.

Among the different works considered for the extraction of stars, a main contribution has been taken from Anthony-Twarog & Twarog (1994), where a calibration of metallicity, and an accurate estimation of the reddening based on the reddening maps of Burstein & Heiles (1984) is presented for a sample of more than 100 stars. The selection of stars of this catalogue has the further advantage that their Strömgren photometry is homogenized. We have also included in our sample most of the giant stars contained in the *Catalogue of Spectroscopic Abundances* (Cayrel et al. 1992) observable from the Observatorio del Teide ($-30° < \delta < +64°$). From the extended work on photoelectric $UBVRIJHK$ photometry of globular cluster red giants summarized by Frogel et al. (1983a,b) we have included 137 stars from various globular clusters (M 3, M 67, M 15, M 13, M 71 and 47 Tuc) measured by Cohen et al. (1978) and Frogel et al. (1979, 1981). We have also included 22 giants measured by Carney (1983a), 27 giants from Arribas & Martínez-Roger (1987b) and 39 giants from Selby et al. (1988).

In summary, the sample consists of approximately 400 stars. The metallicities which will be adopted in the present study are obtained from the *Catalogue of Spectroscopic Abundances* (Cayrel et al. 1992), and from revised photometric calibrations which are scaled to the spectroscopic values compiled in that catalogue. The uncertainty in [Fe/H] for the stars in the sample ranges from 0.15 to 0.3 dex.

The optical photometry which will be used in the forthcoming calibrations was obtained from different sources. The $UBV(RI)$ photometry has been taken mainly from the compilations by Mermilliod & Mermilliod (1994); Lanz (1986); Morel & Magnenat (1978), the *Hipparcos Input Catalogue* (Turon et al. 1993); Carney (1983a,b); Jasniewicz (1982) and Johnson et al. (1966). For the remainder of the stars the sources were the *Bright Star Catalogue* (Hoffleit & Jaschek 1982). The relations provided by Bessel (1983) were used to transform RI photometric data from the Cousins and Kron systems where necessary.

Strömgren photometry was extracted mainly from the homogenized catalogue of Hauck & Mermilliod (1990).

The JHK photometry was specifically measured in this programme for nearly 75% of the stars in the sample; for the remainder of the stars the sources were those quoted above.

Apart from unavoidable contamination, several subgiants have been purposely included in the sample to extend the range of surface gravity in the final calibration. Possibly there are also a small number of horizontal branch stars among the bluest stars of the sample.

A crude estimate of the features of the total sample is revealed in Fig. 1, where we show the location of the stars in the $(B-V):(U-B)$ diagram. The dispersion above the average line of solar abundance stars is caused by the blanketing effect associated with the metal content.

3. The observations

The observations were made over eight different periods distributed all through 1994–1997, with the 1.54 m. Carlos Sánchez Telescope (TCS system).

The procedure adopted during the observations is as follows. Several pairs of calibration stars, one ascending and the other descending, were tracked all through each run over an airmass range 1–2. The reduction procedure consisted of the iterative application of the following equation to the set of calibration stars:

$$m_\lambda = m_{I\lambda} - E_\lambda Z - D_\lambda(UT) + (ZP)_\lambda, \quad (1)$$

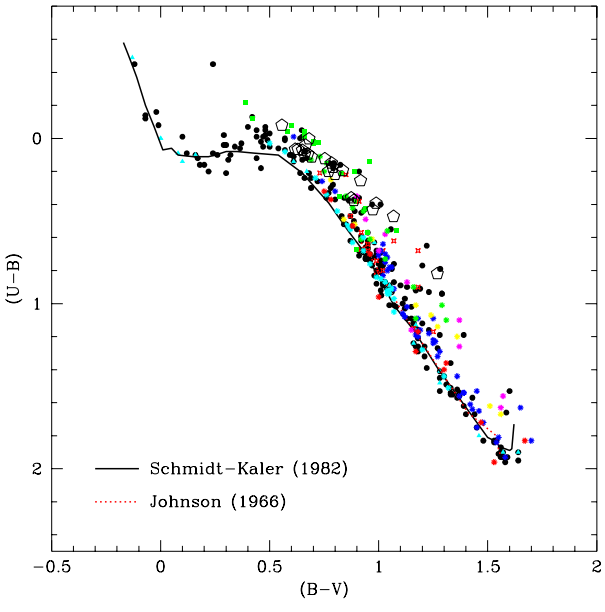

Fig. 1. $(B-V)$ vs. $(U-B)$ for the stars of the sample. The lines show the average fiducial lines for giant stars. The open pentagons show the mean integrated colours of a sample of globular clusters as taken from the data compiled by Peterson (1986)

where m_λ and $m_{I\lambda}$ are respectively the calibration and instrumental monochromatic magnitudes observed for a source star at an airmass Z and time UT, E_λ is the extinction coefficient at wavelength λ, D_λ accounts for the temporal drift, and $(ZP)_\lambda$ is the instrumental zero point. In this way, Bouguer lines were obtained every night. There was a considerable overlap in the standard and programme stars observed in different runs, in order to prevent zero-point differences between them. Two different impedances were used in the amplifier system of the photometer, the low impedance mode was adopted to measure in L' and bright stars ($K \lesssim 4$ mag) in JHK; however the high impedance mode was adopted in JHK measurements for faint stars ($K \gtrsim 3$ mag) in order to minimize the noise. In Table 1, we list the calibration stars observed during the campaign. As can be appreciated, they cover a wide magnitude range (0 mag $\lesssim K \lesssim 8$ mag) and in spectral types (late B to early M) which match properly the composition of our sample. In Table 2 we present the $JHK(L')$ magnitudes of the programme stars (approximately 2500 measurements in JHK and 700 in L' including calibration)[2]. When there were more than two measurements, the $JHKL'$ magnitudes are the average of the observations in each waveband. In Fig. 2, we display the histograms of the residuals of the stars measured more than twice (approximately 75% of the sample). The mean internal consistency of measurements in J, H and K is around 0.02 mag, and $0.03 - 0.04$ mag for L'. The amount of data presented is enough to provide a preliminary qualitative analysis of the extinction in the near-IR bands at the Observatorio del Teide.

In Fig. 3, we show the correlation between the extinction coefficients in the three different bands. The relations are as follows:

$$E_J = 1.172E_H + 0.045 \ \ (\sigma = 0.036) \tag{2}$$

$$E_J = 1.350E_K - 0.003 \ \ (\sigma = 0.035) \tag{3}$$

$$E_{L'} = 0.55E_J + 0.04 \ \ (\sigma = 0.060). \tag{4}$$

We have considered the average of the least squares fits of the x-axis versus the y-axis, and the y-axis versus the x-axis, in order to determine the slope of the linear fit more accurately. The relation in L' is very uncertain because no measurements of $E_{L'}$ were made in high-extinction conditions. The consistency with the previous relations derived in Alonso et al. (1994b; Paper II) is noteworthy. If one adopts extinction in H band as baseline for the comparisons (since this is the cleanest band) then the intercepts in the extinction plots for J and K bands versus H band are positive (as deduced from Eqs. (2) and (3)), which would imply a non-zero aerosol extinction (0.045 mag for J and 0.036 mag for K). As regard L', the intercep has a lesser level of confidence, given that there are no high extinction values of L'. By considering the above relations, the decrease in extinction from $J(1.279\,\mu m)$ to $H(1.648\,\mu m)$ to $K(2.186\,\mu m)$ to $L'(3.690\,\mu m)$ is in the ratio 1.172:1:0.868:0.645. If we fit these data to a law of the form $\lambda^{-\alpha}$, we get $\alpha = 0.60 \pm 0.2$. This value is in agreement with the values quoted by Hayes & Latham (1975) as measured in the optical range in different astronomical observatories, which ranges between $\alpha = 0.5$ and $\alpha = 1.5$.

If we take as fiducial values for the extinction in the near-IR bands between 1 and 2 air masses those reported by Manduca & Bell (1979) and Volk et al. (1989), which would correspond to dust free nights with 2 to 10 mm of precipitable water vapour (i.e. E_J 0.07 − 0.10, E_H 0.04 − 0.06 and E_K 0.05 − 0.08), roughly 35% of the nights are within these conditions (J: 34%, H: 38% and K: 35%). Furthermore, only $\sim$ 20% of the nights show strong extinction ($E > 0.2$ in J, $E > 0.15$ in H and K). As for L', the typical extinction lies within the range 0.07 − 0.15. In general, large extinction values in spring are mainly caused by water vapour absorption; however in summer, they are connected with the dust transported over the observatory by southerly winds from the Sahara desert (an atmospheric phenomenon known locally as *calima*).
In summary, this concise analysis supports the good quality of the Observatorio del Teide for near-infrared observations.

[2] Hereafter L' and L_{TCS} will be equivalently used to denote L' magnitudes measured at the Carlos Sánchez Telescope.

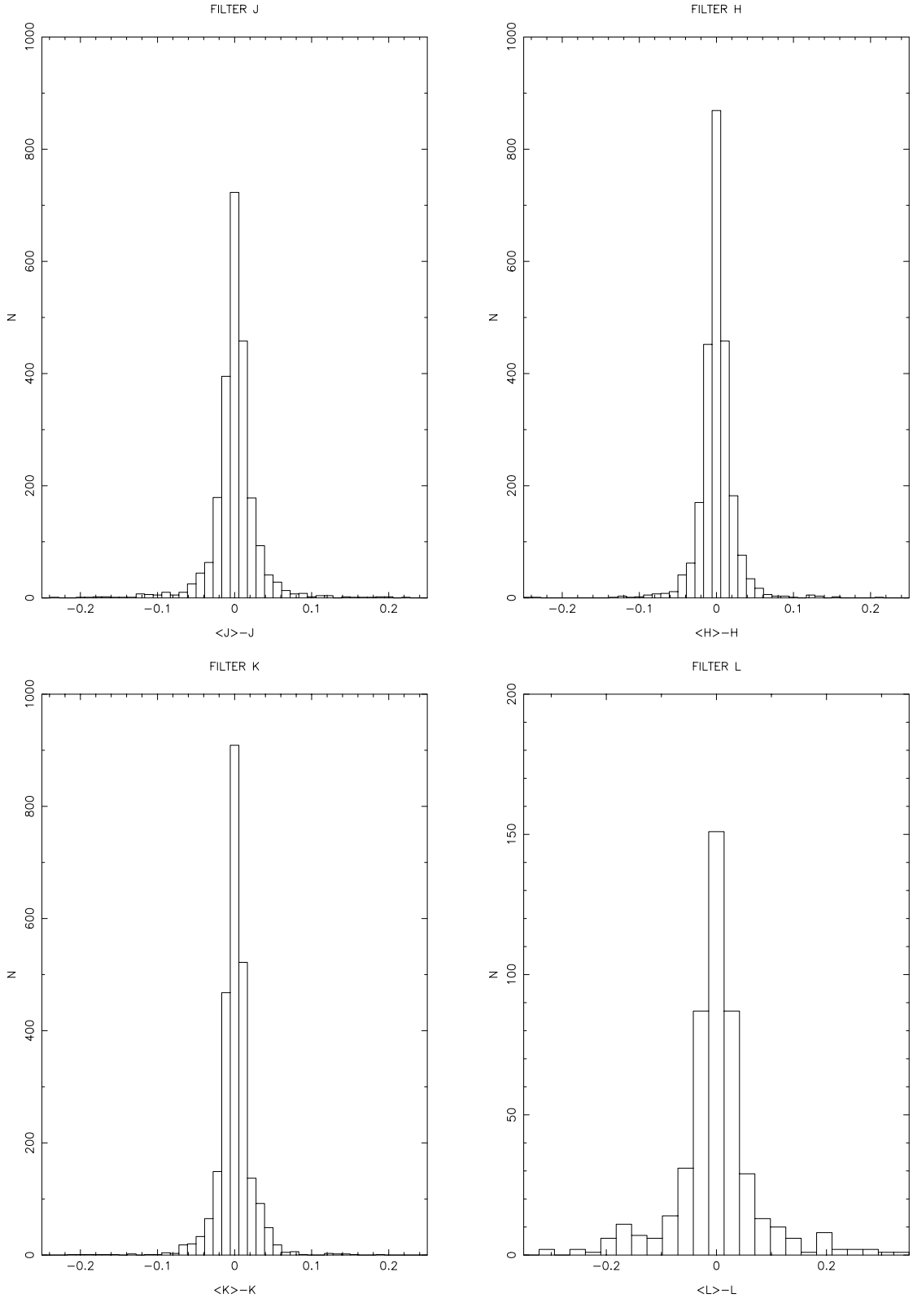

Fig. 2. Residuals of the observed magnitudes in each filter. Note that the axis scales are different for L' according to the small number of measurements made with this filter

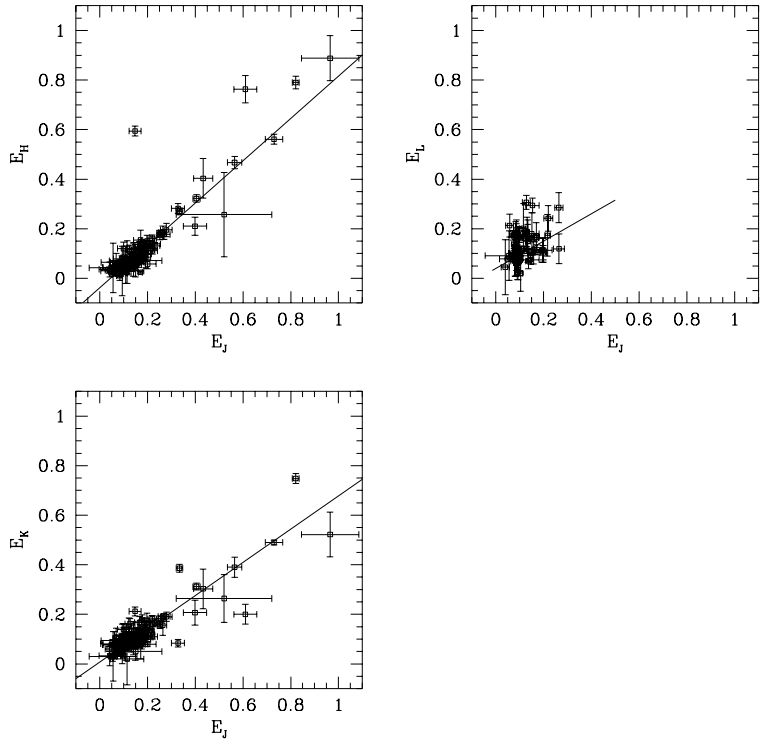

Fig. 3. The correlation between extinction coefficients in the different bands measured at the Observatorio del Teide (TCS System). The straight lines correspond to the fits obtained (Sect. 3). Note the consistency of the relation for high extinction values, this point grants the reliability of colours obtained even in dusty conditions

3.1. Transformations into/from other photometric systems

The differences in the atmospheric transmission at each site and the absence of standard infrared filters make transformation equations necessary in order to homogenize magnitudes measured in different systems. Since the previous work which established the TCS system (Kidger 1992; Alonso et al. 1994a Paper I; and Paper II), we have made an effort to increase the number of stars common with other near-IR photometric systems. For the first time we also include L' magnitudes. We present the re-calculated transformations for magnitudes and colours into/from the systems of Johnson (Johnson et al. 1966; Johnson et al. 1968; Lee 1970), ESO (Bouchet et al. 1991), CIT and Selby et al. (1988) narrow band. It is noteworthy that the ranges of validity of the transformations has been extended in colour. As expected, the dispersion of the correlations has decreased with the increase in the number of stars compared to previous ones. We show the residuals between the transformed and observed TCS magnitudes in order to assess the linearity of the TCS system (Fig. 4). No appreciable departures from zero are noted in the residuals of the transformed magnitudes (except for H values which are probably caused by the somewhat poor definition of this band in the Jonhnson system). This ensures the linearity of the TCS system over the range -3 mag $< K < 10.5$ mag.

3.1.1. Johnson vs. TCS

From a historical point of view the first photometric measurements in the near IR windows were made by Johnson (1966). The large number of measurements of some of his standards makes of this system a necessary reference for comparison. For the definition of H-band of Johnson system we have considered the works by Johnson et al. (1968) and Lee (1970), and the transformations provided by Bessell & Brett (1988). We have made an effort to almost double the number of stars common to both the TCS and the Johnson systems.

$$J_{\rm TCS} = J_{\rm J} - 0.040 - 0.064(J-K)_{\rm J} \quad (\sigma = 0.033; 105 \text{ stars}), \tag{5}$$

$$H_{\rm TCS} = H_{\rm J} - 0.020 - 0.034(J-K)_{\rm J} \quad (\sigma = 0.036; 37 \text{ stars}), \tag{6}$$

$$K_{\rm TCS} = K_{\rm J} - 0.042 + 0.019(J-K)_{\rm J} \quad (\sigma = 0.030; 106 \text{ stars}), \tag{7}$$

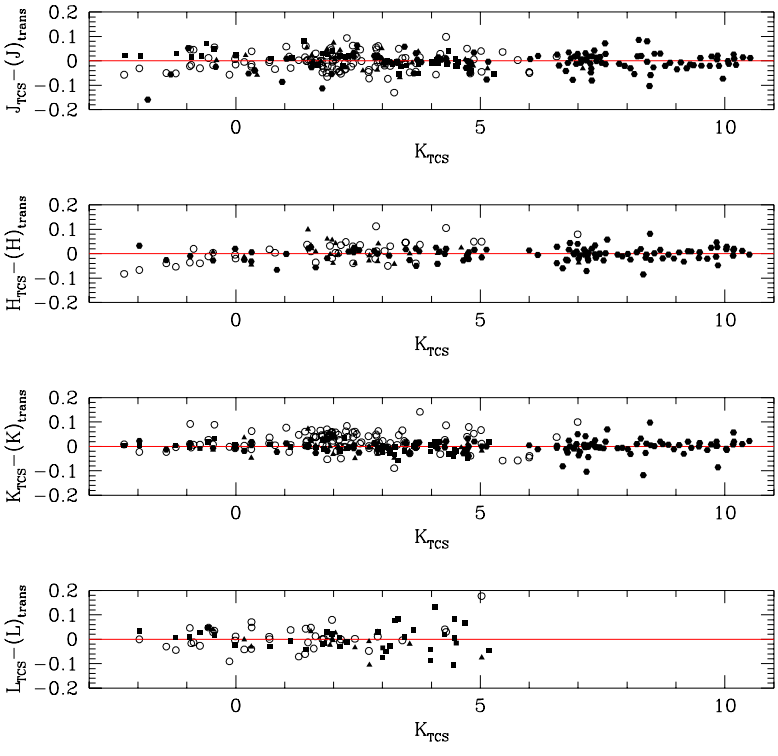

Fig. 4. Residuals of the differences between the magnitudes measured at the Observatorio del Teide, and the magnitudes transformed from the different photometric systems by using the equations of Sect. 3. Open circles: Johnson system; triangles: ESO system; hexagons: CIT system, and squares: Selby et al. (1988)

$$L_{\rm TCS} = L_{\rm J} + 0.04 - 0.016(J-K)_{\rm J} \quad (\sigma = 0.039; 39 \text{ stars}), \tag{8}$$

$$(V-K)_{\rm TCS} = 0.050 + 0.993(V-K)_{\rm J} \quad (\sigma = 0.030; 106 \text{ stars}), \tag{9}$$

$$(J-K)_{\rm TCS} = 0.008 + 0.910(J-K)_{\rm J} \quad (\sigma = 0.030; 106 \text{ stars}), \tag{10}$$

$$(J-H)_{\rm TCS} = -0.010 + 0.942(J-H)_{\rm J} \quad (\sigma = 0.030; 36 \text{ stars}), \tag{11}$$

$$(J-L)_{\rm TCS} = -0.080 + 0.955(J-L)_{\rm J} \quad (\sigma = 0.038; 38 \text{ stars}). \tag{12}$$

These transformations are applicable in the range $-0.2 < (J-K)_{\rm TCS} < 1.2$, $-0.1 < (J-H)_{\rm TCS} < 0.9$, $-0.25 < (J-L)_{\rm TCS} < 1.3$ and $-0.6 < (V-K)_{\rm TCS} < 5.5$.

In order to understand the above transformation equations in terms of the passband profiles available in literature for both the TCS and Johnson systems, we have synthesized IR colours by using Kurucz's models properly sampling gravity, metallicity and effective temperature. For the synthesis of colours we have followed the procedure described in Paper I and Alonso et al. (1995). In Fig. 5, we show the confrontation of the synthetic lines obtained for both systems overimposed on the TCS-colour vs. Johnson-colour diagrams. The mean trends of the synthetic colours reproduce fairly well the loci of the stars considered to establish the transformations, reinforcing the validity of them.

3.1.2. CIT vs. TCS

The CIT system is described in Elias et al. (1982) and Frogel et al. (1978). Carney (1983a,b) also provides a number of stars in this system. The derived equations for magnitudes are:

$$J_{\rm TCS} = J_{\rm CIT} - 0.035 + 0.019(J-K)_{\rm CIT} \quad (\sigma = 0.028; 100 \text{ stars}), \tag{13}$$

$$H_{\rm TCS} = H_{\rm CIT} - 0.025 + 0.030(J-K)_{\rm CIT} \quad (\sigma = 0.020; 100 \text{ stars}), \tag{14}$$

$$K_{\rm TCS} = K_{\rm CIT} - 0.022 + 0.006(J-K)_{\rm CIT} \quad (\sigma = 0.018; (100 \text{ stars}), \tag{15}$$

and the corresponding colour transformations:

$$(J-K)_{\rm TCS} = -0.015 + 1.014(J-K)_{\rm CIT} \quad (\sigma = 0.024; 103 \text{ stars}), \tag{16}$$

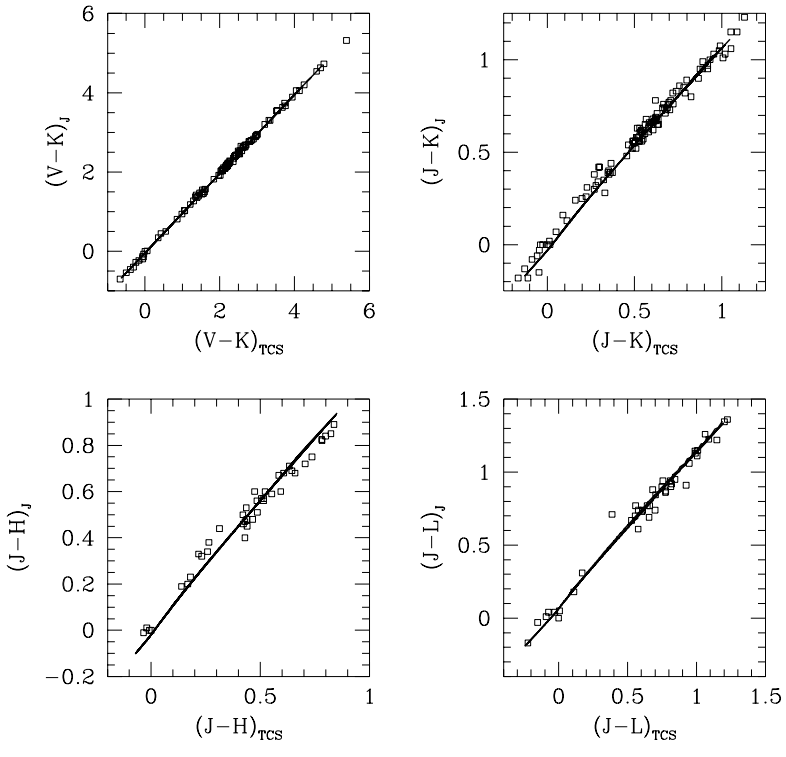

Fig. 5. Infrared colours of the TCS system versus infrared colours of Johnson system. The squares correspond to stars common to both systems. The lines correspond to the synthetic colours obtained by using Kurucz models and the passband of profiles of the filters of each system

$$(J-H)_{\rm TCS} = -0.008 + 0.980(J-H)_{\rm CIT} \quad (\sigma = 0.024; 104 \text{ stars}), \tag{17}$$

$$(V-K)_{\rm TCS} = 0.022 + 0.998(V-K)_{\rm CIT} \quad (\sigma = 0.021; 104 \text{ stars}). \tag{18}$$

The applicability of these transformations is restricted to the following colour ranges: $-0.15 < (J-K)_{\rm TCS} < 1.10$, $-0.08 < (J-H)_{\rm TCS} < 0.85$, $-0.04 < (H-K)_{\rm TCS} < 0.26$, $-1.50 < (V-K)_{\rm TCS} < 6.00$. The transformations to CIT are excellent. The small colour terms and the low dispersion show that both systems share very similar filters. The good agreement with Carney's dwarf data is noteworthy. The slightly high dispersion in J is probably due to the water vapour absorption bands which flank this window.

3.1.3. Narrow-band photometry vs. TCS

Selby et al. (1988) provide high quality photometry for a list of bright stars (measured with a set of narrow-band filters specially designed to avoid the edges of the atmospheric absorption bands and the presence of telluric lines). By using the stars common to both systems we have re-derived the transformations, whose small dispersion reflects the good level of accuracy of the TCS standard system.

$$J_{\rm TCS} = J_{\rm n} - 0.035 + 0.009(J-K)_{\rm n} \quad (\sigma = 0.022; 40 \text{ stars}), \tag{19}$$

$$K_{\rm TCS} = K_{\rm n} - 0.035 + 0.075(J-K)_{\rm n} \quad (\sigma = 0.020; 43 \text{ stars}), \tag{20}$$

$$L_{\rm TCS} = L_{\rm n} + 0.04 + 0.015(J-K)_{\rm n} \quad (\sigma = 0.04; 33 \text{ stars}), \tag{21}$$

$$(V-K)_{\rm TCS} = 0.043 + 0.978(V-K)_{\rm n} \quad (\sigma = 0.020; 43 \text{ stars}). \tag{22}$$

These transformations are applicable in the range $-0.2 < (J-K)_{\rm TCS} < 1.1$, $-0.2 < (J-K)_{\rm TCS} < 1.3$ and $-0.5 < (V-K)_{\rm TCS} < 4.8$.

3.1.4. ESO vs. TCS

Bouchet et al. (1991) have redefined the ESO system after the instrumental change at La Silla. They provide a list of 199 standard stars to an accuracy of 0.02 mag. Given

the importance of comparing TCS system with a southern hemisphere system, we have doubled the number of common stars with respect to Paper II, thereby tightening the relations obtained and extending the colour ranges. The strong colour term for the J transformation, which only can be explained by assuming different effective wavelengths for this band in both systems, is remarkable.

$$J_{\rm TCS} = J_{\rm ESO} - 0.047 - 0.102(J-K)_{\rm ESO} \quad (\sigma = 0.035; 26 \text{ stars}), \tag{23}$$

$$H_{\rm TCS} = H_{\rm ESO} - 0.068 + 0.016(J-K)_{\rm ESO} \quad (\sigma = 0.030; 26 \text{ stars}), \tag{24}$$

$$K_{\rm TCS} = K_{\rm ESO} - 0.042 + 0.006(J-K)_{\rm ESO} \quad (\sigma = 0.028; 26 \text{ stars}), \tag{25}$$

$$L_{\rm TCS} = L_{\rm ESO} + 0.037 - 0.057(J-K)_{\rm ESO} \quad (\sigma = 0.031; 16 \text{ stars}). \tag{26}$$

The transformations for colours are:

$$(V-K)_{\rm TCS} = 0.039 + (V-K)_{\rm ESO} \quad (\sigma = 0.027; 26 \text{ stars}), \tag{27}$$

$$(J-K)_{\rm TCS} = -0.012 + 0.910(J-K)_{\rm ESO} \quad (\sigma = 0.019; 27 \text{ stars}), \tag{28}$$

$$(J-H)_{\rm TCS} = 0.010 + 0.883(J-H)_{\rm ESO} \quad (\sigma = 0.015; 27 \text{ stars}), \tag{29}$$

$$(J-L)_{\rm TCS} = -0.073 + 0.946(J-L)_{\rm ESO} \quad (\sigma = 0.032; 16 \text{ stars}). \tag{30}$$

The applicability of these transformations is restricted to the following colour ranges: $-0.15 < (J-K)_{\rm TCS} < 0.90$, $-0.10 < (J-H)_{\rm TCS} < 0.70$, $-0.9 < (V-K)_{\rm TCS} < 3.5$, and $-0.2 < (J-L)_{\rm TCS} < 1.0$.

3.2. L' bandpass

The transmission of the J, H and K bands has been described in Paper II. Here we present the transmission of the L' filter (Table 3). The experimental arrangement for this measurement was the same as that adopted for the J, H and K filters. Although the L' filter of the TCS system has been somewhat optimized (i.e. it is not so broad as the original L filter of the Johnson system, and partly avoids the most opaque region of the L window), it can be appreciated that it is strongly affected by the water vapour bands absorption which plague this wavelength range. This is why the number of measurements in L' is less than in JHK, as the total number of useful nights is correspondingly smaller. Also for this reason the correlation between extinction in J and L' is somewhat more difficult to establish, as it is mainly related to water vapour absorption instead of the aerosol component. The absolute calibration of the L' (and also that of the JHK) photometry has been linked to Vega (BS7001) following the method described in Paper I.

4. Colour-colour diagrams

In Fig. 6 we show different IR diagrams derived from the data of the present observational programme (given in Table 2). The internal consistency of the derived colours given the small scatter around the average loci in all diagrams (discarding obviously a few individual measurements) is noteworthy. The dispersion in the $(H-K)$ colour may account for an effect of metallicity similar to that found for main sequence stars (Paper II). The similarity between the $(J-L) : (H-L)$ and $(V-K) : (U-V)$ diagrams supports this possibility. The absence of stars at the turn-over of the $(H-K) : (J-H)$ diagram shows that the biasing of the sample with late K and M dwarfs is practically negligible. Discrepancies in the mean trends of solar metallicity lines published by other authors are seen. These could be ascribed partly to the uncertainty of the transformations applied in this work; however, zero-point and/or calibration problems in the definition of those photometric systems should not be completely discarded.

In order to ascertain the influence of metallicity on near–IR colours we have plotted the $(H-K) : (J-H)$ diagram for the whole sample, separating stars in three groups of decreasing metallicity which roughly correspond to the disk, halo/disk transition and halo populations (Fig. 7). The data of each of the groups in the range F5–K2 have been fitted, by using the least–squares method, to straight lines of the form $(H-K) = a + b(J-H)$. The group with $[Fe/H] \geq -0.5$ consists of 140 stars, in this case the fit yields $a = 0.01$ and $b = 0.19$ with a rms error of 0.013 mag. The group with $-0.5 \geq [Fe/H] \geq -1.5$ consists of 84 stars, in this case the fit yields $a = -0.01$ and $b = 0.22$ with a rms error of 0.017 mag. The group with $-1.5 \geq [Fe/H]$ consists of 88 stars, in this case the fit yields $a = -0.02$ and $b = 0.25$ with a rms error of 0.015 mag. It can be appreciated that the slope of the mean traces increases slightly with decreasing metal content. This effect is similar to that found for dwarf stars in Paper II. It is probably related to the ion H^-, which is the dominant source of continuum opacity in the near infrared wavelength range for the spectral types under consideration. Notice that the possible bias of insterstellar reddening can be safely neglected in this analysis, since on the one hand the size of the expected dereddening vectors is small, and on the other, their direction is approximately parallel to the mean traces of the giant stars on the $(H-K) : (J-H)$ diagram.

In Table 4, we provide the computed IR colours in the TCS system according to spectral type and luminosity class. For the computation of the mean colours we have considered the photometric data of stars contained in Paper II and in the present sample with reliable spectral classification.

The interstellar extinction has not been taken into account, however most of the stars considered are population I giants with well determined spectral types which

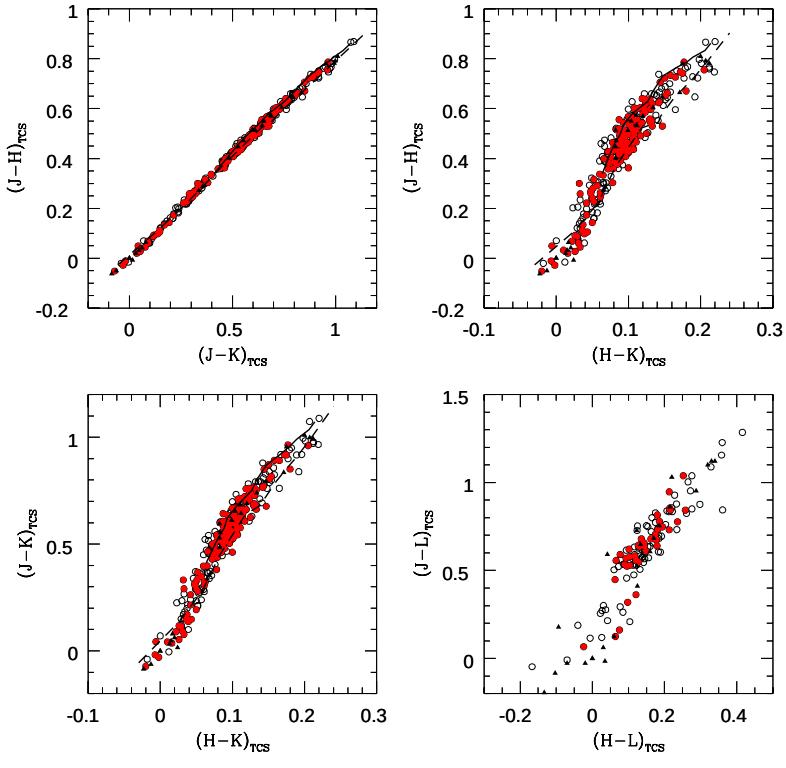

Fig. 6. Infrared colour diagrams for the stars of the sample measured at the Observatorio del Teide. Solid circles : stars measured more than twice; open circles: stars measured once; triangles: TCS standards taken from Kidger (1992). The superimposed lines correspond to the intrinsic relation extracted from literature and transformed to the TCS system. Solid line: Bessel & Brett (1988); dashed line: Bouchet et al. (1991)

Table 4. Computed mean colours in the system of the TCS (Carlos Sánchez Telescope) for giant and main sequence stars, separated according to spectral types

Sp. type	$(J-H)$	$(J-K)$	$(H-K)$	Sp. type	$(J-H)$	$(J-K)$	$(H-K)$
A0III	–0.003	–0.002	0.008	A0V	0.000	0.015	0.015
A4III	0.048	0.064	0.016	A4V	0.032	0.053	0.021
A7III	0.095	0.134	0.038	A7V	0.047	0.061	0.014
F0III	0.132	0.163	0.032	F0V	0.148	0.179	0.033
F2III	0.152	0.192	0.039	F2V	0.153	0.190	0.039
F5III	0.214	0.261	0.047	F4V	0.174	0.219	0.044
F8III	0.331	0.400	0.070	F5V	0.212	0.249	0.036
G0III	0.429	0.515	0.085	F6V	0.242	0.286	0.044
G2III	0.432	0.526	0.085	F7V	0.268	0.318	0.045
G5III	0.448	0.533	0.087	F8V	0.271	0.325	0.050
G7III	0.454	0.542	0.089	F9V	0.294	0.343	0.045
G8III	0.484	0.586	0.097	G0V	0.308	0.352	0.048
K0III	0.521	0.617	0.102	G2V	0.315	0.365	0.050
K1III	0.550	0.655	0.105	G5V	0.330	0.390	0.060
K2III	0.571	0.698	0.125	G8V	0.388	0.461	0.073
K3III	0.616	0.750	0.134	K0V	0.462	0.549	0.088
K4III	0.639	0.775	0.136	K3V	0.496	0.588	0.092
K5III	0.723	0.899	0.179	K5V	0.561	0.683	0.121

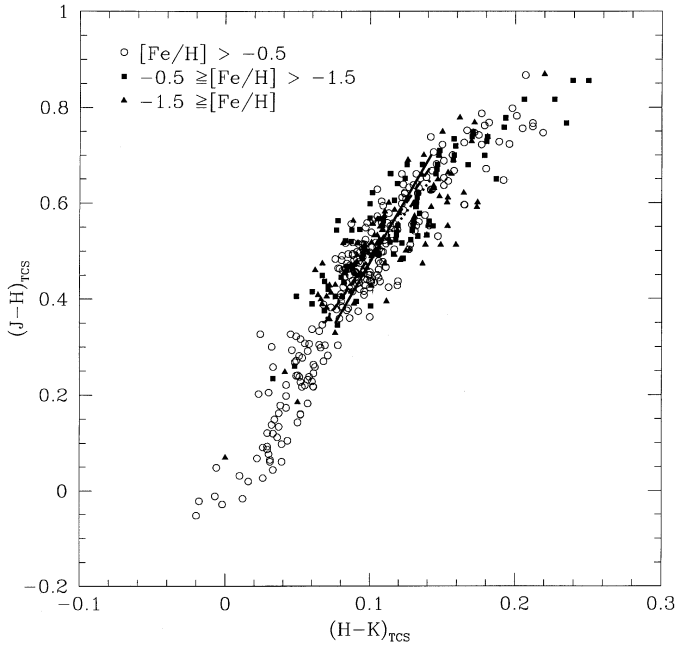

Fig. 7. $(H-K):(J-H)$ diagram for the stars of the whole sample separated according to metallicity. Open circles: [Fe/H] ≥ -0.5 (Disk); squares: $-0.5 \geq$ [Fe/H] ≥ -1.5 (Disk/Halo transition); triangles $-1.5 \geq$ [Fe/H] (Halo). The data in the range F5−K2 have been fitted to straight lines of the form $(J-H) = a + b(H-K)$. The mean lines obtained are overimposed on the graph to show the sensitivity of IR colours to metallicity. Solid line [Fe/H] ≥ -0.5; dashed line $-0.5 \geq$ [Fe/H] ≥ -1.5; dotted line $-1.5 \geq$ [Fe/H]

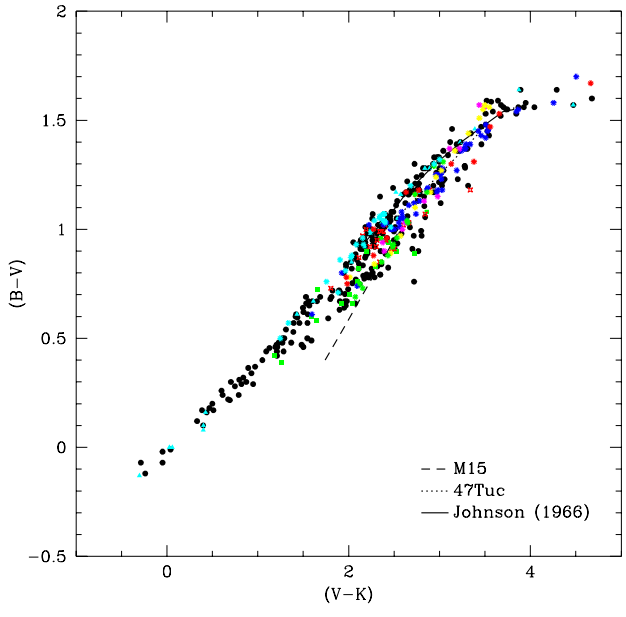

Fig. 8. $(V-K):(B-V)$ diagram for the stars of the sample. The superimposed lines correspond to the intrinsic relation extracted from Johnson (1966) for Population I giants. Black circles correspond to stars with IR colours measured in the present work; the remaining symbols correspond to stars taken from the sources described in Sect. 2. Dotted line: intrinsic line for 47 Tuc (Martínez-Roger 1985). Dashed line: intrinsic line for M 15 (Martínez-Roger 1985)

are close to the solar neighbourhood. We have adopted a rejection criteria in order to calculate the mean values, for this reason the number of stars considered to obtain each colour varies slightly, this is the cause of the small discrepancies observed when adding $(J-H)$ and $(H-K)$ to obtain $(J-K)$. The small differences between the mean lines of giants and dwarfs are significant, indeed both lines should only strongly diverge for types later than K3III $((V-K) > 2.5)$.

Diagrams which combine optical and IR colours are suitable for analysing separately the effects of effective temperature and metallicity. In the $(V-K):(B-V)$ diagram (Fig. 8) the spread under the intrinsic line for population I stars is due mainly to the blanketing effect on the $(B-V)$ colour, since $(V-K)$ is hardly sensitive to metallicity. We show the mean lines for the giant branch of 47 Tuc ([Fe/H] ~ -1) and M 15 ([Fe/H] ~ -2). The different variation of the $(V-K)$ colour with metallicity when compared with that found for dwarf stars, especially in the redder part of the diagrams (see Paper II), is remarkable. In the $(V-K):(U-V)$ diagram (Fig. 9) this point is even more conspicuous than in the $(V-K):(B-V)$ diagram, although a considerable number of stars in our sample lack U measurements. In this case, the stretching of the metallicity axis is larger, since the blanketing effects in the U band are stronger. Superimposed on the sample stars we show, for the sake of comparison, the intrinsic lines for 47 Tuc (Frogel et al. 1981), typical for disc globular clusters, and the average for M 3, M 13, and M 92 (Cohen et al. 1978) as representative of halo globular clusters. It is clear from this point that the different Galactic populations of giant stars are well represented.

5. Summary

We present the result of a long-term observational programme of IR photometry for an extended sample of giant stars. The analysis of colour-colour diagrams shows that the target of selecting a sample which covers the metallicity range found in our Galaxy has been properly accomplished. The JHK photometry is accurate to 0.02 mag and the L' photometry to $0.03 - 0.04$ mag. These levels of accuracy will allow the determination of effective temperatures for the sample stars within and error of 1.5% by applying the Infrared Flux Method.

As a complementary result the new IR photometry has allowed an extension and improvement in the characterization of the TCS photometric system.

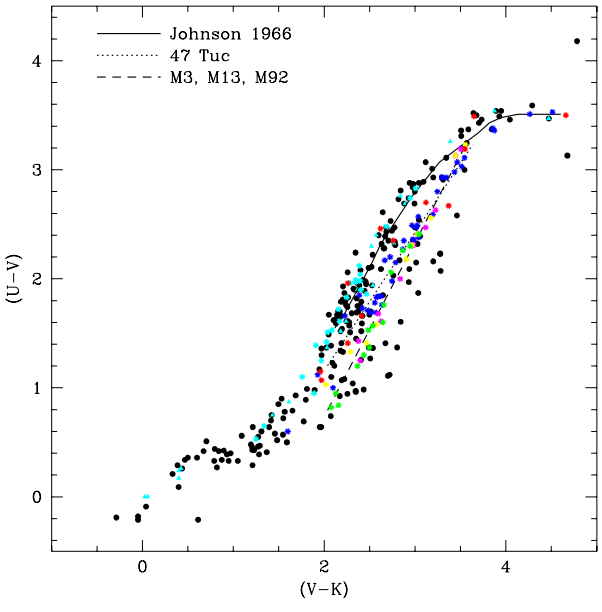

Fig. 9. $(V-K) : (U-V)$ diagram for the stars of the sample. The superimposed lines correspond to the intrinsic relation extracted from Johnson (1966) for Population I giants. Black circles correspond to stars with IR colours measured in the present work; the remining symbols correspond to stars taken from the sources described in Sect. 2. This diagram provides an instructive characterization of the sample insofar as the $(V-K)$ axis reflects the extension in temperature, and the $(U-V)$ axis the blanketing effect associated with the metal abundance of stars

Acknowledgements. Based on observations made with the Carlos Sánchez Telescope of the Observatorio del Teide (Tenerife), operated by the Instituto de Astrofisica de Canarias. We are grateful to Terry Mahoney for the careful reading of the manuscript.

References

Alonso A., Arribas S., Martínez-Roger C., 1994a, A&A 282, 684 (Paper I)
Alonso A., Arribas S., Martínez-Roger C., 1994b, A&AS 107, 365 (Paper II)
Alonso A., Arribas S., Martínez-Roger C., 1995, A&A 297, 215
Alonso A., Arribas S., Martínez-Roger C., 1996a, A&AS 117, 227 (Paper III)
Alonso A., Arribas S., Martínez-Roger C., 1996b, A&A 313, 873 (Paper IV)
Anthony-Twarog B.J., Twarog B.A., 1994, AJ 107, 1577
Arribas S., Caputo F., Martínez-Roger C., 1991, A&AS 88, 19
Arribas S., Martínez-Roger C., 1987a, A&A 178, 107
Arribas S., Martínez-Roger C., 1987b, A&AS 70, 303
Bell R.A., Gustafsson B., 1989, MNRAS 236, 653
Bell R.A., 1992, MNRAS 257, 423
Bessell M.S., 1983, PASP 95, 480
Bessell M.S., Brett J.M., 1988, PASP 100, 1134, 1983, PASP 95, 480
Blackwell D.E., Petford A.D., Arribas S., Haddock D.J., Selby M.J., 1990, A&A 232, 396
Bonifacio P., Molaro P., 1997, MNRAS 285, 847
Bouchet P., Manfroid J., Schmider F.X., 1991, A&AS 91, 409
Burstein D., Heiles C., 1982, AJ 87, 1165
Carney B.W., 1983a, AJ 88, 610
Carney B.W., 1983b, AJ 88, 623
Castelli F., Gratton R.G., Kurucz R.L., 1997, A&A 318, 841
Cayrel de Strobel G., Hauck B., François T., et al., 1992, A&AS 95, 273
Cohen J.G., Frogel J.A., Persson S.E., 1978, ApJ 222, 165
Elias J.H., Frogel J.A., Matthews K., Neugebauer G., 1982, AJ 87, 1029
Frogel J.A., Persson S.E., Aaronson M., Matthews K., 1978, ApJ 220, 75
Frogel J.A., Persson S.E., Cohen J.G., 1979, ApJ 227, 499
Frogel J.A., Persson S.E., Cohen J.G., 1981, ApJ 246, 842
Frogel J.A., Persson S.E., Cohen J.G., 1983a, ApJ 275, 773
Frogel J.A., Persson S.E., Cohen J.G., 1983b, ApJS 53, 713
Hauck B., Mermilliod M., 1990, A&AS 86, 107
Hayes D.S., Latham D.W., 1975, ApJ 197, 593
Hoffleit D., Jaschek C., 1982, The Bright Star Catalogue. Yale University Observatory, New Haven
Jasniewicz G., 1982, A&AS 49, 99
Johnson H.L., 1966, ARA&A 4, 193
Johnson H.L., Mitchell R.I., Iriarte B., Wisniewski W.Z., 1966, Comm. Lun. Planet. Lab. Nr. 63
Johnson H.L., McArthur J.W., Mitchell R.I., 1968, ApJ 152, 465
Kidger M., 1992, Calibration star programme results, Carlos Sánchez Telescope Technical Note Series, Supplement to Technical Note 16
King J.R., 1994, AJ 107, 1165
Lanz T., 1986, A&AS 65, 195
Lee T.A., 1970, ApJ 162, 217
Manduca A., Bell R.A., 1979, PASP 91, 848
Martínez-Roger C., 1985, PhD Thesis, Universidad de la Laguna
Mermilliod J.C., Mermilliod M., 1994, Catalogue of Mean UBV Data on stars. Springer, New York
Morel M., Magnenat P., 1978, A&AS 34, 477
Peterson C.J., 1986, PASP 98, 192
Selby M.J., Hepburn I., Blackwell D.E., et al., 1988, A&AS 74, 127
Turon C., Egret D, Gómez A., et al., 1993, Hipparcos Input Catalogue (Version 2), ESA SP-1196
Vazdekis A., Casuso E., Peletier R.F., Beckman J.E., 1996, ApJS 106, 307
Volk K. Clark T.A., Milone E.F., 1989, in Lecture Notes in Physics, Infrared Extinction and Standardization, Proceedings, Baltimore, MD 1988, Milone E.F. (ed.). Springer, p. 15